Journal of Power Sources 185 (2008) 1499–1504

Contents lists available at ScienceDirect

Journal of Power Sources

journal homepage: www.elsevier.com/locate/jpowsour

Electrochemical characterisation of activated carbon particles used in redox flow battery electrodes

G.J.W. Radford[a,1], J. Cox[a], R.G.A. Wills[b], F.C. Walsh[b,*]

[a] Regenesys Technologies Limited, Harwell, United Kingdom
[b] Electrochemical Engineering Laboratory, Energy Technology Research Group, School of Engineering Sciences, University of Southampton, Highfield, Southampton SO17 1BJ, United Kingdom

ARTICLE INFO

Article history:
Received 20 December 2007
Received in revised form 21 July 2008
Accepted 3 August 2008
Available online 20 August 2008

Keywords:
Activated carbon
Electrochemical treatment
Electrochemical properties
Porosity
Porous carbon

ABSTRACT

The Faradaic and non-Faradaic characteristics of a series of activated carbon particles (used to produce composite carbon–polymer electrodes for redox flow cells) have been determined using aqueous electrolytes (sulfuric acid and sodium polysulfide) at 295 K. The particles were mounted as a circular section (ca. 0.80 cm^2) shallow packed bed of 2.5 mm thickness in the direction of electrolyte flow (mean linear flow velocity $\approx 6\,mm\,s^{-1}$). Cyclic voltammetry in deaerated, 1 mol dm^{-3} H_2SO_4 at 295 K indicated a specific capacitance in the range of 50–140 F g^{-1}. Linear sweep voltammetry and galvanostatic step studies in an alkaline sodium polysulfide electrolyte (1.8 mol dm^{-3} $Na_2S_{2.11}$) have demonstrated marked differences amongst various types of activated carbon. Such differences are highlighted during galvanostatic charge–discharge cycling of half-cell electrodes in the polysulfide electrolyte. The electrochemical characteristics are compared to those based on (N_2 adsorption) gas porosimetry measurements.

1. Introduction

1.1. Porous carbons

Porous carbons [1] are often used as electrode materials due to their high surface area, good electrical conductivity and relative inertness. Such materials are available in diverse forms, ranging from discrete particles to monolithic foam and felt structures [2,3]. More recently, carbon nanotubes, especially single walled carbon nanotubes (SWCTs) have been intensively studied, e.g. [4,5] but such materials suffer the disadvantages of very high cost, difficulties in preparation, problems in the reproducibility of surface structure/chemistry and limited purity. These drawbacks might limit larger scale, technological applications of SWCTs.

Activated carbon particles are widely used as sorbents; in addition to a high surface area, the materials show a microporous structure, the ability to adsorb a wide spectrum of species and a high adsorption capacity together with a high surface reactivity. Such properties have been exploited in electrosorption experiments, where a bed of activated carbon particles (or felt) under potentiostatic control can be used to remove metal ions or dissolved organic species [6–8]. Activated carbon particles have been extensively characterised in terms of the carbon surface, pore size distribution and activity, e.g. [9,10] and electrodes for filter-press cells (including redox flow cells) can be manufactured from activated carbon–polymer particles [11]. The present study seeks to characterise activated carbon particles for particular electrochemical applications, such as redox energy storage using redox flow cells [12]. A laboratory, shallow packed bed reactor is used to screen the performance of the carbons for the sulfide/polysulfide redox reaction.

1.2. Faradaic and non-Faradaic processes

The Faradaic and non-Faradaic characteristics of a range of activated carbon materials can be considered in terms of the active surface of an electrode. Three important cases can be identified:

1.2.1. Electrolyte/solid interface

One limit is the area estimated via double layer capacitance measurements. These measurements correspond to the entire solid surface in contact with the electrolyte solution. The area values obtained may include contributions from some of the smallest pores within the carbon structure.

* Corresponding author. Tel.: +44 2380 598752; fax: +44 2380 598754.
E-mail address: F.C.Walsh@soton.ac.uk (F.C. Walsh).
[1] Current address: St John's College, Grove Road South, Southsea, Hampshire PO5 1QW, United Kingdom.

0378-7753/$ – see front matter © 2008 Elsevier B.V. All rights reserved.
doi:10.1016/j.jpowsour.2008.08.020

Nomenclature

A	electrode area (cm^2)
A_S	specific surface area of the electrode ($cm^2\ g^{-1}$)
c_b	bulk concentration of reactant ($mol\ cm^{-3}$)
C_A	capacitance per unit electrode area ($F\ cm^{-2}$)
C_S	specific capacitance ($F\ g^{-1}$)
D	diffusion coefficient of electroactive species ($cm^2\ s^{-1}$)
E	electrode potential (V)
F	Faraday constant (=96,485 $C\ mol^{-1}$) ($C\ mol^{-1}$)
I	current (A)
I_L	limiting current (A)
$I_{L,S}$	specific limiting current ($A\ g^{-1}$)
I_S	specific (charging) current ($A\ g^{-1}$)
j	current density ($A\ cm^{-2}$)
j_S	specific current density ($A\ cm^{-2}\ g^{-1}$)
R_e	electrical resistance (Ω)
t	time (s)
w	mass of carbon (g)
z	number of electrons in the electrode process

Greek letters

δ_N	Nernst diffusion layer thickness (cm)
η	overpotential (V)
ν	linear potential sweep rate ($V\ s^{-1}$)

1.2.2. Mass transport limited area

The active area for a reaction under mass transport control occurs for either a reaction with rapid kinetics or when a large overpotential is applied such that electron transfer is very rapid. For simple electrode reactions, the surface area can be calculated, under complete mass transport controlled conditions, via the limiting current due to convective-diffusion, I_L which is given by:

$$I_L = k_m A z F c_b = \frac{D A z F c_b}{\delta_N} \quad (1)$$

where k_m is the mass transport coefficient, A the electrode area, F the Faraday constant and c_b is the bulk concentration of reactant. The value of I_L obtained critically depends on the surface roughness of the electrode and the thickness of the mass transport layer. If the surface roughness is small compared to the thickness of the Nernst diffusion layer, δ_N, the area measured will be equal to the geometric area. If the size of the surface roughness of the electrode is similar to the thickness of the diffusion layer, however, surface areas larger than the geometric value will be observed [1]. The thickness of the diffusion layer depends on the experimental conditions (such as the relative electrode/electrolyte flow, electrolyte composition and temperature) but it is normally in the range of 100–1000 μm. In the case of a three-dimensional electrode having a uniform electrode area, Eq. (1) can be rewritten as an expression for the specific limiting current, i.e. the limiting current for a unit weight of electrode material, via:

$$I_{L,S} = k_m A_S z F c_b \quad (2)$$

where A_S is the specific electrode area, i.e., the electrode area per unit weight of electrode material.

1.2.3. Electrochemically active area

The 'electrochemically active' area, i.e. the area of the electrode surface that is active in supporting a charge transfer controlled reaction is very sensitive to the electrode potential. Part of the internal pore surface becomes active and the active zone may vary with the reaction type and the process conditions.

1.3. The aqueous polysulfide/sulfide redox couple

This redox couple has shown promise for energy conversion in photoelectrochemical cells and in redox flow batteries for energy storage [12–17]. The redox couple is also important in pulp and paper processing [18–20]. The polysulfide/sulfide redox reaction in aqueous alkali is a complex process where the sulfur species depend on pH and composition. The reversible reduction of polysulfide ions to sulfide ions can be simplified to:

$$S_4^{2-} + 4H_2O + 6e^- \leftrightarrow 4HS^- + 4OH^- \quad (3)$$

Following a thermodynamic consideration of the chemical speciation involved [13], this reaction has been considered [14] as a solution phase chemical equilibrium between polysulfide and supersulfide ions:

$$S_4^{2-} \leftrightarrow 2S_2^- \quad (4)$$

followed by a heterogeneous electrochemical process to reduce the supersulfide ion to the bisulfide ion:

$$2S_2^- + 4H_2O + 6e^- \leftrightarrow 4HS^- + 4OH^- \quad (5)$$

During potential step experiments in previous studies [14], a second cathodic reaction was evident at higher overpotentials (where an electrochemical reaction preceded a chemical one (i.e., an *EC* mechanism). This reaction was less prominent at lower overpotentials or when the concentration of S_2^- was higher. The study of reaction (5) at a low overpotential proved difficult due to the extremely low currents observed at non-porous electrodes [14]. The *CE* reaction is believed to occur at a very slow rate, making it nearly invisible at common, two-dimensional laboratory electrodes.

In the present paper, the polysulfide/sulfide reaction is simply considered as a reversible, two-electron reduction of the polysulfide anion:

$$S_4^{2-} + 2e^- = 2S_2^{2-} \quad (6)$$

High surface area activated carbons were employed in an attempt to compensate for the low rate of the *CE* reaction and to help identify the critical factors affecting the performance of candidate electrode materials for redox flow cells and other electrochemical power sources. A thin-layer packed bed electrode cell was developed as a rapid tool for the screening of activated carbon particles used as a raw material for planar, moulded carbon–polymer composite electrodes. Such materials have been used to manufacture carbon–polymer composite materials for use as bipolar electrodes in redox flow batteries [11,12,17]. The objective of the present study was to provide a rapid screening technique to evaluate activated carbon powders used in the manufacture of carbon–polymer composite electrodes for redox flow batteries. A number of RFB technologies are under development for energy storage and load levelling applications [12].

2. Experimental details

2.1. The porous, packed bed electrode cell

A 'flow-through' packed bed reactor (Fig. 1) was used for estimating double layer capacitance values via cyclic voltammetry and galvanostatic step experiments. A shallow, cylindrical bed of carbon particles (with a circular cross-sectional area of 80 mm^2 and thickness of 2.5 mm) was placed in contact with a platinum mesh current feeder and compressed between two, highly porous, glass sinters. A

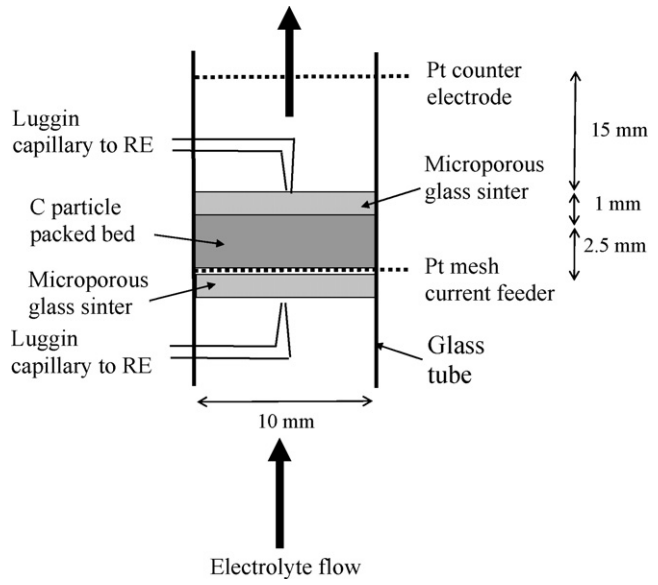

Fig. 1. Schematic of the 'flow through' packed bed electrode for electrochemical evaluation of activated carbon particles.

constant mean linear electrolyte velocity of 6 mm s^{-1} through the bed was employed. Double layer capacitance measurements were made at 295 ± 2 K in 1 mol dm^{-3} sulfuric acid or potassium chloride solution (each electrolyte being deoxygenated by a fast stream of nitrogen gas prior to testing).

The arrangement used for Faradaic studies consisted of a standard, three-compartment glass electrochemical cell. A single layer of activated carbon particles was attached to an insulated graphite rod current feeder (0.79 cm^2) using a thin layer of conductive carbon cement. The electrolyte was agitated at a constant rate using a magnetic stirrer. During potential step experiments, the potential of the working electrode was recorded *vs.* a saturated calomel electrode (SCE) and controlled via a computer controlled potentiostat (Windsor Scientific, Autolab). Faradaic reactions were studied in aqueous 1.8 mol dm^{-3} $Na_2S_{2.11}$ polysulfide at 295 ± 2 K. The electrolyte was prepared by addition of sulfur to an alkaline, 1.8 mol dm^{-3} solution of Na_2S in 1 mol dm^{-3} KOH solution, followed by electrolysis to produce the required level of polysulfide ion.

2.2. The activated carbon particles

Activated carbon materials having a broad range of physical properties were supplied by Sutcliffe Speakman Carbons Ltd. The proprietary materials had been activated using a variety of oxidative techniques. The pore size distribution of each material was determined using the classical techniques of N_2 sorption and Hg porosimetry as summarised in Table 1. 203C, 207C and AR1 carbons were all produced from coconut precursors with an increasing degree of activation. 208EA material was produced from a coal-based compound while DCL was a lignite coal derivative. Unactivated coconut shell, UNCS carbon was also used for the purpose of comparison.

The nitrogen adsorption data show that the total surface area of the coconut carbons increased at higher degrees of activation. The results also suggest that the 208EA carbon possessed a surface area similar to that of the 207C whilst the DCL carbon had a higher surface area which is close to that of the AR1 sample. Mercury porosimetry again showed an increase in porosity with the degree of activation for coconut shell carbons. The results suggested that the surface area of the 208EA was similar to that of AR1 and that the DCL carbon possessed a much greater pore volume than the other carbons. Whereas nitrogen adsorption is able to characterise the micro-, meso- and macro-porosity of the carbon, mercury porosimetry can only provide information concerning meso- and macro-porosity [21].

3. Results and discussion

3.1. Non-Faradaic processes

Cyclic voltammetry was carried out in aqueous sulfuric acid (1 mol dm^{-3}, 295 K, flow rate 6 mm s^{-1}) at controlled potential sweep rates using a packed bed reactor. The capacitance per unit area can be estimated from the charge envelope under the cyclic

Table 1
Physical properties of the activated carbon particles studied

	Type of activated carbon particles					
	UCNS	203C	207C	AR1	208EA	DCL
Precursor	Coconut shell	Coconut shell	Coconut shell	Coconut shell	Bituminous coal	Lignite coal
Sample description	Unactivated	Medium activity	High activity	High activity	Broad pores; high activity carbon	Low density; broad pores
Specific surface area (N_2 gas) (m^2 g^{-1})	652	380	1010	1530	1070	1400
Total specific pore volume (N_2 gas) (cm^3 g^{-1})	–	0.19	0.46	0.79	0.49	1.0
Specific micropore volume (N_2 gas) (cm^3 g^{-1})	0.29	0.17	0.43	0.71	0.46	0.71
Total specific pore volume (liquid Hg) (cm^3 g^{-1})	0.21	0.16	0.32	0.44	0.43	1.11
Specific mesopore volume (liquid Hg) (cm^3 g^{-1})	0.08	0.07	0.13	0.27	0.23	0.44
Specific macropore volume (liquid Hg) (cm^3 g^{-1})	0.12	0.09	0.19	0.17	0.20	0.68

N_2 gas refers to nitrogen gas adsorption at 77 K (total pore volumes are defined as: micropore 0–2 nm width, 0–20 nm width, narrow micropore 0–06 nm width, broad micropore 0.6–2 nm width. Liquid Hg refers to mercury porosimetry at 297 ± 2 K (total pore volumes are defined as: 2–10 nm width, mesopore volume 2–50 nm width, macropore volume 50–10^4 nm width [27]).

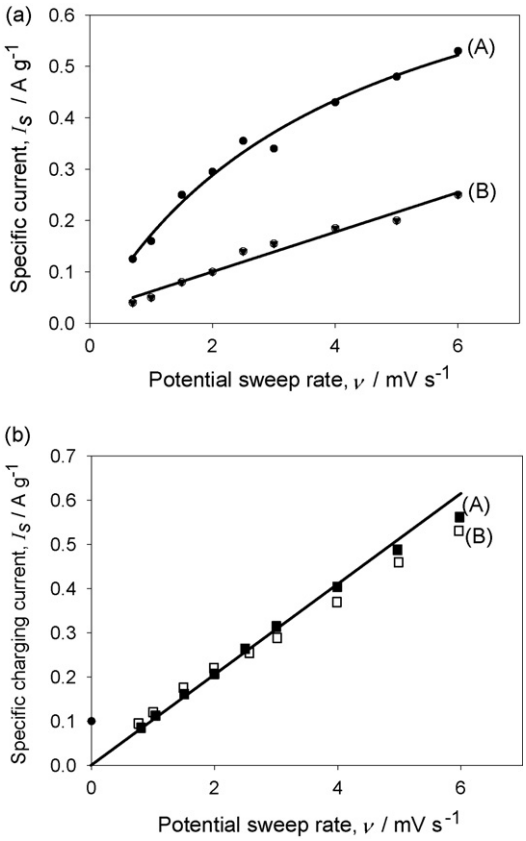

Fig. 2. Charging current *vs.* potential sweep rate for beds of dried carbons in 1 mol dm^{-3} sulfuric acid at 295 K. (a) The behaviour of (A) 207C activated carbon and (B) unactivated coconut shell carbon (UCNS) particles. (b) Two beds of dried, activated 207C carbon particles (A) bed 2 and (B) bed 1.

voltammogram in potential regions were no Faradaic current was observed. The current density is then given by:

$$j = C_A \nu \tag{7}$$

where C_A is the capacitance per unit area of the activated carbon and ν is the linear potential sweep rate (dE/dt).

When a charging current or a change in potential addresses a practical porous electrode, the available electrode area is not charged at a uniform rate due to a non-uniform reaction environment. As a result, capacitance values will be higher at the lower sweep rates and the slope of the plot of specific current *vs.* potential sweep rate decreases with increasing sweep rate. The specific capacitance, C_S may be related to the current density, j by:

$$C_S = \frac{jA}{w\nu} = \frac{j_S A}{\nu} \tag{8}$$

where j_S is the specific current density. From the plot of the specific charging current *vs.* potential sweep rate shown in Fig. 2(a), specific capacitance values of 53 and 84 F g^{-1} were calculated for UCNS and 207C activated carbon, respectively, These values correspond to approximately 40% of the maximum theoretical value of 130 F g^{-1}, assuming a capacitance of 20 μF cm^{-2} and a BET surface area of 652 m^2 g^{-1} for the unactivated coconut shell carbon.

The effect of drying the 207C activated carbon (at 100 °C for 5 h) resulted in a 15% decrease in weight. A plot of the specific charging current *vs*. the potential sweep rate for the dried 207C particles is shown in Fig. 2(b). A marked increase in the specific capacitance from 84 to 144 F g^{-1} was observed compared to the 'as-received' material. This increase may result from the combined

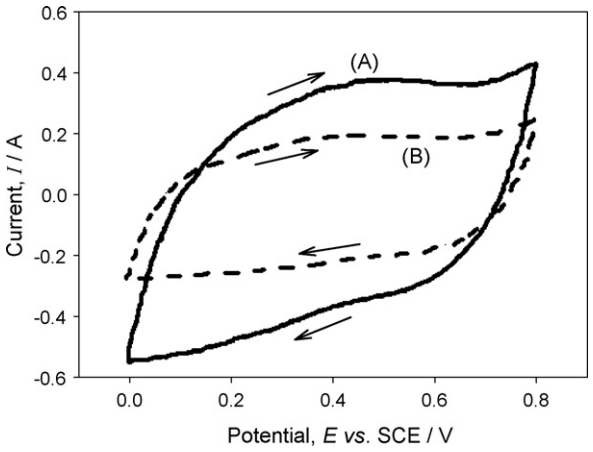

Fig. 3. Cyclic voltammograms for (A) 1.503 g and (B) 0.750 g of 207C activated carbon beds in 1 mol dm^{-3} sulfuric acid at 295 K using a potential sweep rate of 2 mV s^{-1}.

effect of the reduced weight per volume of activated carbon and the subsequent ingress of electrolyte within those pores previously containing absorbed moisture. The value of 144 F g^{-1} is consistent with literature values of 120–160 F g^{-1} [15] for activated carbon in 1 mol dm^{-3} sulfuric acid (Chemviron RC carbon with a BET surface area of 1100–1300 m^2 g^{-1}). The double layer capacitance of planar carbon electrodes in aqueous media is typically 20 μF cm^{-2} and 207C activated carbon has a BET surface area of 1041 m^2 g^{-1} resulting in a maximum theoretical capacitance of approximately 200 F g^{-1}. Activated carbons contain micropores of less than 2 nm diameter, however, that may not be fully wetted by the electrolyte.

Fig. 3 illustrates the reduction in electrical charge (equivalent to the area under the curve of current *vs.* potential plots) as a result of the reducing the mass of carbon particles. The specific capacitance was again calculated to be approximately 140 F g^{-1}. In potassium chloride solution, a capacitance value of 90 F g^{-1} was determined by cyclic voltammetry, compared to 140 F g^{-1} in sulfuric acid under similar conditions. These values agree well with data presented in the literature from a study of nanoporous carbons (obtained by selective leaching of titanium and aluminium from Ti_2AlC and boron from B_4C), where values for the specific capacitance were found to be between 52 and 125 F g^{-1} [22]. The capacitance of the

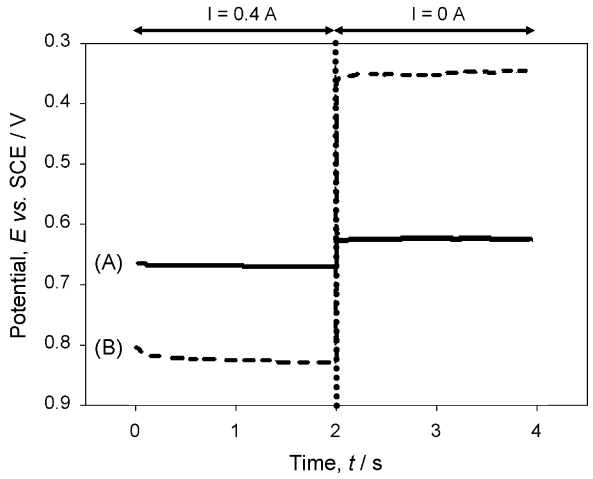

Fig. 4. Potential *vs.* time curves for a bed of 207C activated carbon in 1 mol dm^{-3} sulfuric acid at 295 K with the reference electrode (A) adjacent to the Pt current feeder and (B) adjacent to the activated carbon bed. The current was switched from 0.4 A to 0 A at t = 2 s.

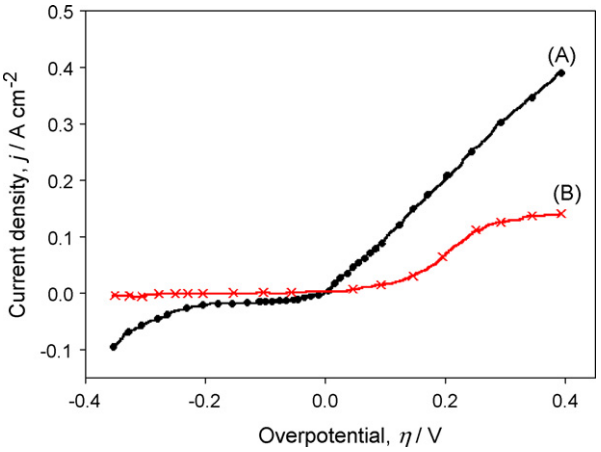

Fig. 5. Potential step experiments (10–20 mV steps at 100 s intervals) in a polysulfide electrolyte (1.8 mol dm^{-3} $Na_2S_{2.11}$ aqueous solution) at 295 K. (A) 207C activated carbon particles and (B) two-dimensional graphite particles.

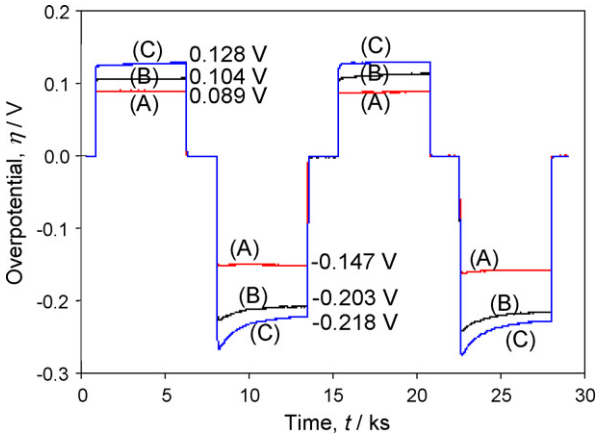

Fig. 6. Overpotential *vs.* time for various activated carbon particles during galvanostatic cycling at a current density of ±250 mA cm^{-2}. (A) 207C (R_e = 0.16 Ω), (B) DCL lignite carbon (R_e = 0.19 Ω) and (C) 208EA coal-based carbon (R_e = 0.18 Ω).

activated carbon depends on the nature of the adsorbed ion. It is believed that the sulfate ion exists as $[SO_4^{2-}(H_2O)_{12}]$ with an associated diameter of approximately 5.3 Å. A pore size of around two to three times that of the electrolyte complex has been considered necessary to achieve a high capacitance [23,24]. The sulfate ion can be accommodated inside the micropores (which have a diameter <2.0 nm) within the activated carbon surface.

In galvanic experiments, the ohmic resistance of the cell was determined using a current interrupt, chronopotentiometric method (within a time interval of 0.5 ms). A constant current was applied for a controlled period. The current was then switched off, followed by discharge of the double layer. Linear extrapolation of the current *vs.* time curve to a time equal to zero allowed the *IR* drop to be calculated and the uncompensated resistance established [25].

Fig. 4 illustrates a typical potential *vs.* time curve obtained for 207C activated carbon. The experiment involved application of a 0.4 A current through the activated carbon particle bed for 2 s followed by switching to open-circuit. Potentials were measured via matching reference electrodes (SCEs) placed above and below (adjacent to Pt current feeder) the activated carbon bed; as shown by the upper and lower luggin capillaries in Fig. 1. The average resistance, obtained with the reference electrode located adjacent to the current feeder, was calculated to be 0.11 ± 0.01 Ω. This was significantly lower than the resistance value measured with the reference located at above the bed (1.28 ± 0.02 Ω). Overpotentials of ±100 mV were subsequently applied to the packed bed and the current was monitored with time (not shown). The rate was clearly lower for the reference electrode placed above the bed, resulting from the higher bed resistance. The R_eC time constants for a positive potential step were calculated as 25–31 s; values of 280–470 s were obtained when the reference electrode was adjacent to the current feeder (and above the bed). The large variation for the latter condition is due to the difference in resistance between the two beds.

The specific capacitance can also be determined via the charging current, *I* [26]:

$$I = \frac{\Delta E}{R_e} \exp\left(-\frac{t}{R_e C}\right) \quad (9)$$

where ΔE is the potential step, R_e the electrical resistance, t the time and C is the capacitance. Values for the R_eC time constant were estimated from the slope of a semilogarithmic plot of I *vs.* t (not shown) and average values for specific capacitance were typically 150 ± 12 F g^{-1}. The high capacitance values, compared to those obtained via cyclic voltammetry, may be due to Faradaic reactions, such as oxygen evolution, occurring as a result of the initially high currents and hence high potential drop within the bed. Similar values were recorded during negative potential step experiments.

Cyclic voltammetry in 1 mol dm^{-3} sulfuric acid showed that the currents per unit cross-sectional bed area, produced at a non-porous graphite packed bed were approximately 5000 times higher than those experienced at a polished, glassy carbon disc electrode, highlighting the large specific surface area of activated carbons. As expected, the capacitative currents produced were significantly lower than those for the porous carbons. Oxidation/reduction peaks were observed at 0.40 and 0.35 V *vs.* SCE, respectively, at the graphite particles, due to the presence of oxygen functional surface groups on the graphite surface which arise from the process conditions used to manufacture the carbon.

Table 2
Cathodic current densities at an overpotential of −0.2 V and pore volumes for a range of activated carbons particles measured in a polysulfide electrolyte at 295 K

Particulate carbon material	Current density[a] (mA cm^{-2}) (overpotential = 0.2 V)	Specific mesoporosity[b] (cm^3 g^{-1})	Specific macroporosity[c] (cm^3 g^{-1})	Total specific pore volume[d] (cm^3 g^{-1})
203C	1	0.06	0.08	0.14
207C	8	0.12	0.19	0.31
AR1	21	0.26	0.17	0.43
208EA	18	0.23	0.20	0.43
DCL	31	0.43	0.67	1.10

[a] Current density is based on the circular cross-sectional area of the particulate bed.
[b] Mesoporosity is defined (IUPAC) as pores in the size range of 2–50 nm [27].
[c] Macroporosity is defined as pores of size >50 nm [27].
[d] Total specific pore volume is the sum of specific mesoporosity and specific macroporosity.

3.2. Faradaic processes

Repetitive potential step experiments (10–20 mV at 100 s intervals) were performed at the carbon materials within the aqueous polysulfide electrolyte using a three-compartment cell. Fig. 5 clearly demonstrates that the extremely low rate of the *CE* chemical–electrochemical reaction at the graphite particle electrode results in an insignificant cathodic response at low overpotentials. At the porous 207C activated carbon, increased currents are observed which are limited by the supersulfide radical in solution as predicted by Lessner et al. [14]. A second cathodic reaction was evident at higher overpotentials (where an electrochemical reaction precedes a chemical one, *EC*). The anodic reaction rate also appeared to be enhanced by the high internal porosity.

Further evaluation of various activated carbons (having a broad range of physical parameters) was carried out to determine the properties which control electrochemical activity. During potential step experiments, an increase in current was observed with increasing pore volume and (especially) mesopore volume. This was more prominent during the second cathodic excursion (Table 2) due to the increased concentration of reactant at the activated carbon surface as a result of the positive (anodic) potential step. The variation in anodic current density at an overpotential of 0.2 V further demonstrated a significant pore volume dependence. The electrochemical activity clearly increased at higher meso/macroporosity levels.

Constant current cycling of a packed bed reactor containing various activated carbon particle beds supported the above data. Fig. 6 shows overpotential *vs.* time profiles during the constant current charging and discharging of three types of activated carbon particles. The overpotentials recorded for the DCL lignite coal-based carbon particles were smaler than those at 208EA of lower meso/macroporous volume. The performance of the carbons was completely independent of microporosity when using both techniques.

4. Conclusions

1. Very large specific capacitance values were recorded for the activated carbons when compared to non-porous and unactivated materials, suggesting that all but the small micropores were utilised. The specific capacitance varied with background electrolyte.
2. Faradaic reactions involving the aqueous polysulfide/sulfide redox couple indicated that an increased rate was observed as a consequence of the presence of porosity. A smaller fraction of the real surface area appears active and electrochemical conversion is likely to occur in the larger meso/macropores.
3. Under the experimental conditions, several activated carbons showed a relatively high specific mesoporosity and a high electrochemical activity for the reduction of the polysulfide ion. Such electrode materials have found use as planar, carbon–polymer composite bipolar electrodes in redox flow batteries.

Acknowledgements

Activated carbon particles were supplied by Sutcliffe Speakman Ltd. (which is now a part of the Chemviron Carbon organisation (http://sutcliffespeakman.com/homefrmr.htm).

References

[1] F.C. Walsh, A First Course in Electrochemical Engineering, The Electrochemical Consultancy, Romsey, 1993.
[2] D. Pletcher, F.C. Walsh, in: J.D. Genders, N.L. Weinberg (Eds.), Electrochemical Technology for a Cleaner Environment, Electrosynthesis Company Inc., Lancaster, NY, 1993, pp. 51–100.
[3] D. Pletcher, F.C. Walsh, Industrial Electrochemistry, 2nd ed., Chapman-Hall, London, 1992.
[4] K.H. An, K.K. Jeon, W.S. Kim, Y.S. Park, S.C. Lim, D.J. Bae, J. Kor. Phys. Soc. 39 (2001) S511–S517.
[5] G. Girishkumar, K. Vinodgopal, P.V. Kamat, J. Phys. Chem. B 108 (2004) 19960–19966.
[6] S.Y. Qian, B.E. Conway, G. Jerkiewicz, Phys. Chem. Chem. Phys. 1 (1999) 2805–2813.
[7] A. Afkhami, B.E. Conway, J. Colloid Interf. Sci. 251 (2002) 248–255.
[8] J. Niu, B.E. Conway, J. Electroanal. Chem. 546 (2003) 59–72.
[9] Z. Li, M. Kruk, M. Jaroniec, S.K. Ryu, J. Colloid Interf. Sci. 204 (1998) 151–156.
[10] F. Julien, M. Baudu, M. Mazet, Water Res. 32 (1998) 3414–3424.
[11] T.J. Calver, S.E. Male, P.J. Mitchell, I. Whyte, US Patent 6,511,767, January 28, 2003, assigned to Regenesys Technologies Limited.
[12] C. Ponce de León, A. Frias-Ferrer, J. González-Garcia, D.A. Szánto, F.C. Walsh, J. Power Sources 160 (2006) 716–732.
[13] P.M. Lessner, F.R. McLarnon, J. Winnick, E.J. Cairns, J. Electrochem. Soc. 140 (1993) 1847–1849.
[14] P.M. Lessner, F.R. McLarnon, J. Winnick, E.J. Cairns, J. Appl. Electrochem. 22 (1992) 927–934.
[15] A. Price, S. Bartley, S. Male, G. Cooley, Power Eng. J. 13 (3) (1999) 122–129.
[16] P.J. Morrissey, P.J. Mitchell, D.A. Szánto, N.J. Ward, International Patent: WO 02/71522 A1 (2002).
[17] F.C. Walsh, Pure Appl. Chem. 73 (12) (2001) 1819–1837.
[18] M. Behm, D. Simonsson, J. Appl. Electrochem. 27 (1997) 507–528.
[19] I.C. Hamilton, R. Woods, J. Appl. Electrochem. 13 (1983) 783–790.
[20] G.M. Dorris, Pulp Paper Can. 95 (1994) T394–T399.
[21] K.K. Unger, J. Rouqerol, K.S.W. Sing, H. Krai (Eds.), Characterisation of Porous Solids, Elsevier, Amsterdam, 1988.
[22] J. Chmiola, G. Yushin, R.K. Dash, E.N. Hoffman, J.E. Fischer, M.W. Barsoum, Electrochem. Solid State Lett. 8 (7) (2005) A357–A360.
[23] K. Kinoshita, Carbon, Electrochemical and Physicochemical Properties, Wiley, 1988, p. 441.
[24] D. Pletcher, A First Course in Electrochemical Processes, The Electrochemical Consultancy Ltd., Romsey, 1991, p. 86.
[25] M. Endo, T. Maeda, T. Takeda, Y.J. Kim, K. Koshiba, H. Hara, M.S. Dresselhaus, J. Electrochem. Soc. 148 (2001) A910–A914.
[26] T. Balduf, G. Valentin, F. Lapicque, in: F. Lapicque, et al. (Eds.), Electrochemical Engineering and Energy, Plenum Press, New York, 1995, p. 104.
[27] J. Rouquerol, D. Avnir, C.W. Fairbridge, D.H. Everett, J.H. Haynes, N. Pernicone, J.D.F. Ramsay, K.W.S. Sing, K.K. Unger, IUPAC, Pure Appl. Chem. 66 (8) (1994) 1739.